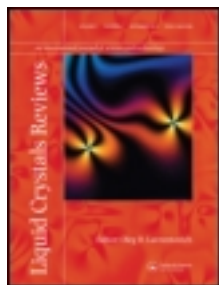


This article was downloaded by: [Université Paris-Sud]

On: 18 February 2014, At: 04:24

Publisher: Taylor & Francis

Informa Ltd Registered in England and Wales Registered Number: 1072954 Registered office: Mortimer House, 37-41 Mortimer Street, London W1T 3JH, UK



Liquid Crystals Reviews

Publication details, including instructions for authors and subscription information:

<http://www.tandfonline.com/loi/tlcr20>

Liquid-crystalline properties of aqueous suspensions of natural clay nanosheets

E. Paineau^a, A.M. Philippe^b, K. Antonova^c, I. Bihannic^d, P. Davidson^a, I. Dozov^a, J.C.P. Gabriel^e, M. Impéror-Clerc^a, P. Levitz^f, F. Meneau^g & L.J. Michot^f

^a Laboratoire de Physique des Solides, UMR 8502, Université Paris-Sud, Bâtiment 510, 91405 Orsay Cedex, France

^b Laboratoire d'Energétique et de Mécanique Théorique et Appliquée, Université de Lorraine - CNRS, UMR 7563, 2 Avenue de la Forêt de Haye, TSA 60604, 54518 Vandoeuvre CEDEX, France

^c Institute of Solid State Physics, Bulgarian Academy of Sciences, Boulevard Tzarigradsko Chaussee 72, 1784 Sofia, Bulgaria

^d Laboratoire Environnement et Minéralurgie, UMR 7569, Nancy University, BP 40, 54501 Vandoeuvre Cedex, France

^e DSM/DPNS, CEA, 17, rue des Martyrs, 38054 Grenoble cedex, France

^f Physico-chimie des Electrolytes, Colloïdes et Sciences Analytiques UMR 7195 - UPMC - CNRS - ESPCI, UPMC bâtiment F, 4 place Jussieu, 75252 Paris Cedex 5, France

^g Synchrotron SOLEIL, L'Orme des Merisiers, Saint-Aubin, BP 48, 91192 Gif-sur-Yvette Cedex, France

Published online: 28 Nov 2013.

To cite this article: E. Paineau, A.M. Philippe, K. Antonova, I. Bihannic, P. Davidson, I. Dozov, J.C.P. Gabriel, M. Impéror-Clerc, P. Levitz, F. Meneau & L.J. Michot (2013) Liquid-crystalline properties of aqueous suspensions of natural clay nanosheets, *Liquid Crystals Reviews*, 1:2, 110-126, DOI: [10.1080/21680396.2013.842130](https://doi.org/10.1080/21680396.2013.842130)

To link to this article: <http://dx.doi.org/10.1080/21680396.2013.842130>

PLEASE SCROLL DOWN FOR ARTICLE

Taylor & Francis makes every effort to ensure the accuracy of all the information (the "Content") contained in the publications on our platform. However, Taylor & Francis, our agents, and our licensors make no representations or warranties whatsoever as to the accuracy, completeness, or suitability for any purpose of the Content. Any opinions and views expressed in this publication are the opinions and views of the authors, and are not the views of or endorsed by Taylor & Francis. The accuracy of the Content should not be relied upon and should be independently verified with primary sources of information. Taylor and Francis shall not be liable for any losses, actions, claims, proceedings, demands, costs, expenses, damages, and other liabilities whatsoever or howsoever caused arising directly or indirectly in connection with, in relation to or arising out of the use of the Content.

This article may be used for research, teaching, and private study purposes. Any substantial or systematic reproduction, redistribution, reselling, loan, sub-licensing, systematic supply, or distribution in any form to anyone is expressly forbidden. Terms & Conditions of access and use can be found at <http://www.tandfonline.com/page/terms-and-conditions>

Liquid–crystalline properties of aqueous suspensions of natural clay nanosheets[†]

E. Paineau^a, A.M. Philippe^b, K. Antonova^c, I. Bihannic^d, P. Davidson^{a*}, I. Dozov^a, J.C.P. Gabriel^e, M. Impéror-Clerc^a, P. Levitz^f, F. Meneau^g and L.J. Michot^f

^aLaboratoire de Physique des Solides, UMR 8502, Université Paris-Sud, Bâtiment 510, 91405 Orsay Cedex, France; ^bLaboratoire d’Énergétique et de Mécanique Théorique et Appliquée, Université de Lorraine – CNRS, UMR 7563, 2 Avenue de la Forêt de Haye, TSA 60604, 54518 Vandœuvre CEDEX, France; ^cInstitute of Solid State Physics, Bulgarian Academy of Sciences, Boulevard Tzarigradsko Chaussee 72, 1784 Sofia, Bulgaria; ^dLaboratoire Environnement et Minéralurgie, UMR 7569, Nancy University, BP 40, 54501 Vandœuvre Cedex, France; ^eDSM/DPNS, CEA, 17, rue des Martyrs, 38054 Grenoble cedex, France; ^fPhysico-chimie des Electrolytes, Colloïdes et Sciences Analytiques UMR 7195 - UPMC - CNRS - ESPCI, UPMC bâtiment F, 4 place Jussieu, 75252 Paris Cedex 5, France; ^gSynchrotron SOLEIL, L’Orme des Merisiers, Saint-Aubin, BP 48, 91192 Gif-sur-Yvette Cedex, France

(Received 1 July 2013; final version received 4 September 2013)

Clay minerals, like beidellite or nontronite, spontaneously exfoliate in water and form colloidal suspensions of nanosheets. In a given range of concentration, these suspensions display a nematic liquid–crystalline phase whose structure and properties can be conveniently studied in detail by polarized-light microscopy and small-angle X-ray scattering (SAXS). Moreover, *in situ* SAXS investigations of sheared clay suspensions provide information about their flow properties, both in the isotropic and nematic phases. The colloidal nematic phase shows the classical properties of usual nematics, such as surface anchoring and electric-field and magnetic-field alignment. Thus, nematic single domains can be produced. The isotropic phase also displays strong electro-optic effects in moderate electric fields. Finally, we describe a few examples of applications of such systems and we show how these studies could be extended to suspensions of other types of nanosheets.

Keywords: liquid crystals; clays; colloids; nanosheets; suspensions; nematic

1. Introduction

The recent worldwide development of the field of mineral or synthetic nanoparticles has sparked renewed interest in colloidal suspensions. From a theoretical point of view, these suspensions allow studying statistical physics issues such as crystallization or the glass transition on length and time scales much larger, and therefore more accessible, than those involved in atomic or molecular systems. From an applied point of view, preparing colloidal suspensions could represent a major step towards easier processing of nanoparticles into films, fibres, or even metamaterials. Among all the nanoparticles described to date, a fair amount is intrinsically anisotropic so that nanotubes, nanorods, nanoribbons, nanodisks, and nanosheets are now widely available. In agreement with statistical physics models and numerical simulations, colloidal suspensions of anisotropic building blocks, whatever their chemical nature, may spontaneously organize in liquid–crystalline phases, as is now well documented for various systems.[1,2] This naturally also applies to mineral nanoparticles whose suspensions form different mesophases (nematic, smectic, and columnar) often called “mineral liquid crystals”.[3,4]

Among all kinds of anisotropic nanoparticles, nanosheets are presently attracting more and more interest. (Here, we call “nanosheet” two-dimensional crystallites of sub-micronic diameter and of well-defined, small, thickness comparable to the unit-cell size.) For example, thanks to its peculiar physical properties, graphene has recently been the focus of intense experimental and theoretical studies.[5,6] Consequently, graphene and graphene oxide suspensions have been produced and shown to display a liquid–crystalline nematic phase.[7–13] Colloidal suspensions of nanosheets can conveniently be produced by exfoliation of low-dimensional layered materials. Large numbers of such solid-state compounds were synthesized in the last decades for many industrial applications such as batteries. They are also widely found in nature, like clay minerals.

Aqueous colloids of natural clay minerals are one particularly good example of nanosheet suspension that has been much studied in the recent years. Indeed, apart from their utmost relevance in geosciences, clay minerals are used in numerous industrial applications including cosmetics, food industry, civil engineering, paints, oil-drilling industry, etc.

*Corresponding author. Emails: patrick.davidson@u-psud.fr, davidson@lps.u-psud.fr

[†]This article is dedicated to the memory of Prof. Christophe Baravian who passed away at the beginning of December 2012 at the age of 44. This work is based on many of the ideas he developed all along his too-short career.

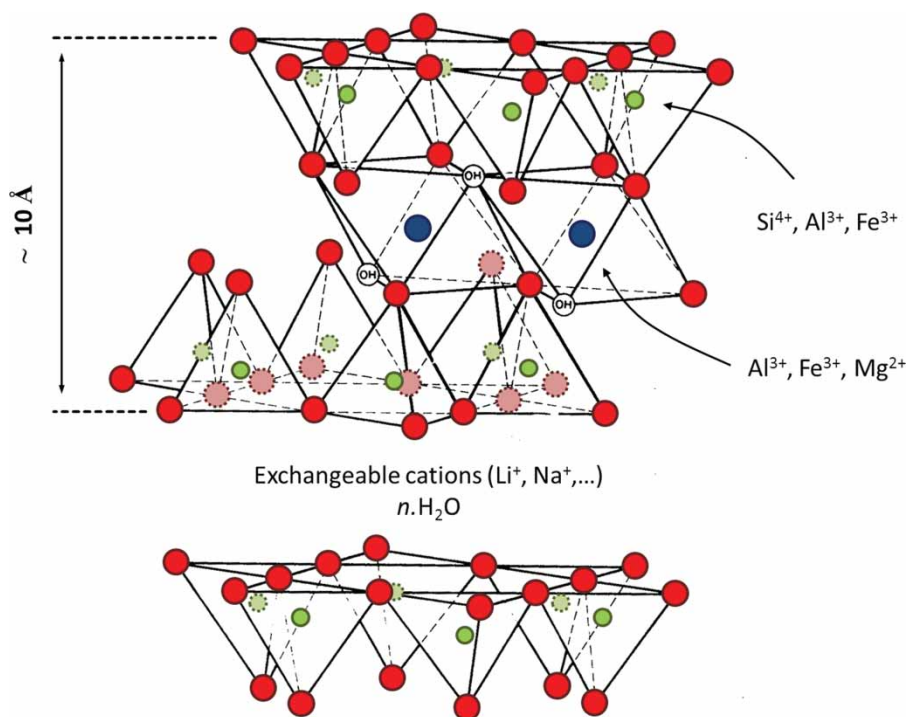


Figure 1. Crystal structure of a dioctahedral smectite nanosheet (adapted from Grim [21]).

The field of natural clays is extremely wide and diverse and we will here restrict the topic to the class of the so-called “swelling clays” or smectites, thus excluding rod-like and tube-like clays even though the colloidal suspensions of such objects, like sepiolite, imogolite, or attapulgite, also display interesting liquid–crystalline phases.[14–20]

Figure 1 shows the generic atomic structure of a clay nanosheet.[21] For swelling clays of the “TOT” type described in the present article, the nanosheet is made of a central octahedral layer sandwiched between two tetrahedral layers. In the case of smectites, the clay sheet bears a negative electrical charge because atomic substitutions occur either in the tetrahedral layers or in the octahedral one.

The charge location of various standard natural smectites is represented in Figure 2.[22] As will be shown below, the colloidal suspensions of some of these clay minerals (Figure 2, red symbols) display liquid–crystalline phases, whereas the suspensions of some others (Figure 2, blue symbols) only form physical gels. Since their early reports [23,24] by Freundlich in 1928 and by Langmuir in 1938, clay gels have been investigated extensively because they provide relevant model systems to study jamming and arrested states in colloidal suspensions.[25–40] In spite of this large body of work, the precise nature of these gels is still debated to date. This issue is clearly related to the complexity of electrostatic interactions between charged anisotropic objects in aqueous solvents. From the point of view of the liquid–crystalline properties, the existence of this gelation phenomenon is essentially a nuisance as it restricts the domain of stability of the nematic phase.

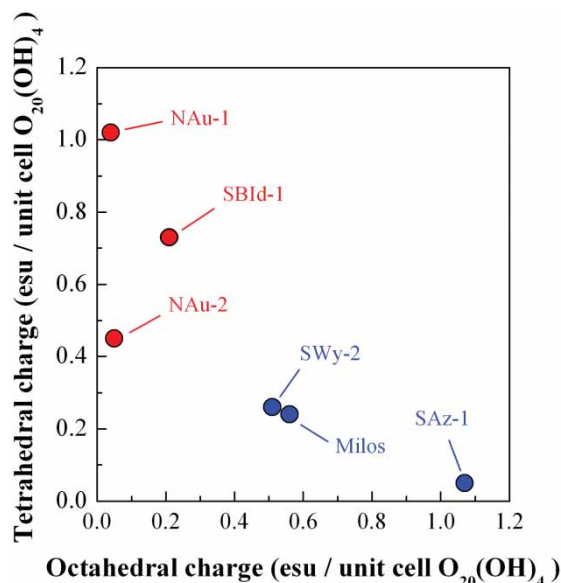


Figure 2. Comparison of the charge location (tetrahedral versus octahedral) for different reference smectite clays (colour online only).

Note: Nontronites: NAu-1 and NAu-2 (Australia); Beidellite: SBI-1 (Idaho, USA); Montmorillonites: SWy-2 (Wyoming, USA), SAz-1 (Arizona, USA), Milos (Greece).

2. Preparation of colloidal suspensions of clay nanosheets

We now describe how colloidal aqueous suspensions of clay nanosheets are produced. The preparation process starts with purchasing samples of clay minerals from well-known

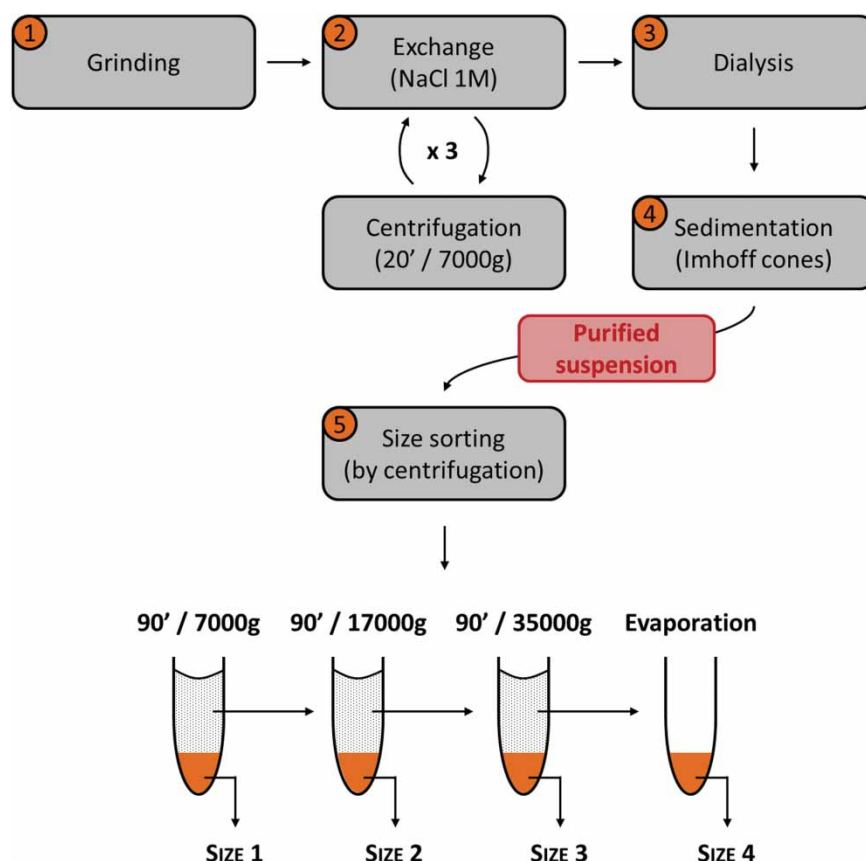


Figure 3. Typical procedure for purification and size fractionation of smectites samples.

clay repositories such as the Source Clays Minerals Repository (Purdue University, USA). This allows working with well-identified samples that were already chemically characterized and ensures both the reproducibility of experiments and the direct comparison of results obtained by different experimental teams. Apart from obvious economic reasons, one interest of working with natural clays instead of synthetic nanosheets is that clay minerals have been weathered for millions of years, which gives them excellent chemical stability in usual conditions.

A typical, well-established, preparation consists in the following steps (Figure 3).[41] The raw clay material is first ground and suspended in water. This suspension is exchanged three times in a NaCl (1 M) solution during 24 h. Then, excess chloride is removed by dialyzing the suspension against Milli-Q water until its conductivity drops below $5 \mu\text{S}/\text{cm}$. The suspension is then poured into Imhoff cones and left to sediment during 24 h. The sediments are then discarded as they contain various impurities. This step ends the purification process. Next, size fractionation procedures, based on successive centrifugations at increasing accelerations and re-dilutions, are used to reduce size polydispersity, resulting in several fractions of decreasing average platelet size. Nevertheless, the analysis of transmission electron

microscopy (TEM) images shows that the nanosheet polydispersity in diameter remains rather high, of the order of 30–40% (Figure 4). Note that particular attention should be given to the determination of platelet diameter, D , because it governs the phase diagram boundaries.[42] In contrast, the nanosheets are most often perfectly exfoliated so that the platelet thickness, t , is about 0.7 nm, with almost no polydispersity. At this stage, the purity of the clay colloid can be checked by X-ray diffraction and infrared spectroscopy, and the nominal electric charge per unit surface (of the order of 0.1 C m^{-2}), independent of particle size, can be estimated by measuring the cationic exchange capacity.

Then, homogeneous suspensions of various compositions are prepared by osmotic stress in order to map out the phase diagram as a function of clay volume fraction and ionic strength. Samples are dialysed against Polyethyleneglycol (PEG, $M_w = 20,000 \text{ g mol}^{-1}$) of known osmotic pressures. Moreover, the ionic strength of the PEG solutions is fixed by adding sodium (or lithium) chloride at different molarities. These solutions are renewed every two weeks, and the dialysis is completed after about one month. Using such a procedure, the final ionic strength of the clay suspensions is fixed without any difficulties related to the Donnan effect.

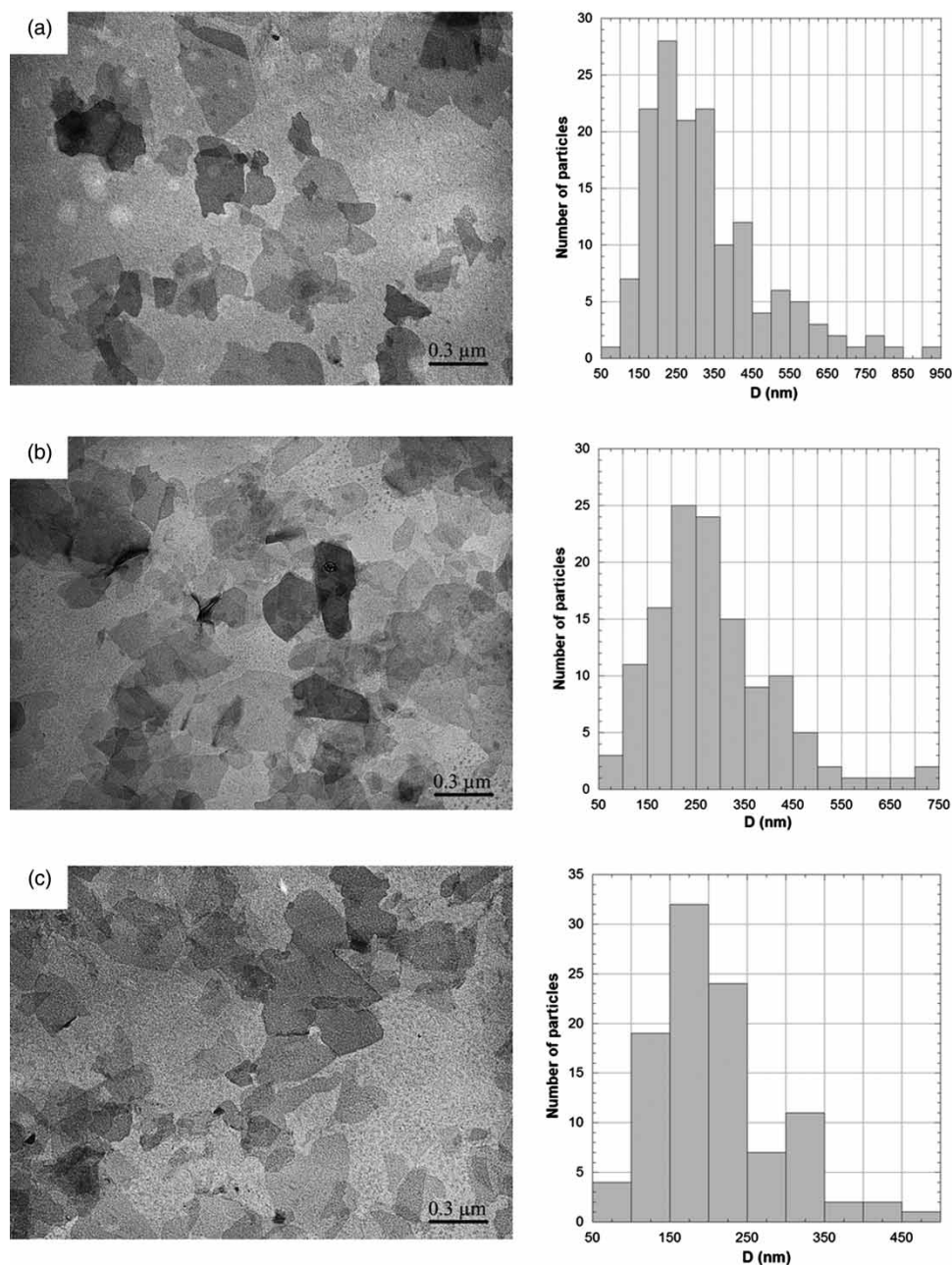


Figure 4. TEM micrographs and diameter distribution histograms of beidellite nanosheets after size fractionation. (a) Size 1; (b) Size 2; and (c) Size 3.

In a last step, the clay suspensions are recovered and their mass concentrations are determined by weight loss upon drying, taking into account the relative humidity according to the water adsorption isotherm of Nasonite.[43] The volume fractions, ϕ , of the suspensions are then calculated using the clay density.

3. Mesomorphism of clay suspensions

In a first step, the simplest method to study the phase behaviour of colloidal suspensions of nanosheets is to

examine samples in test-tubes. For example, Figure 5 shows a series of test-tubes filled with the same amounts of aqueous clay suspensions of increasing volume fractions, observed between crossed polarizers.[41,44,45] Some of these suspensions clearly demix into a birefringent phase at the bottom and an isotropic phase at the top. Moreover, the interface between these two phases moves when the sample is tilted. Such spontaneous phase separation is clear evidence that the samples reach thermodynamic equilibrium and are not trapped in arrested (gel or glass) states. It is the sign of a first-order isotropic to liquid-crystalline phase

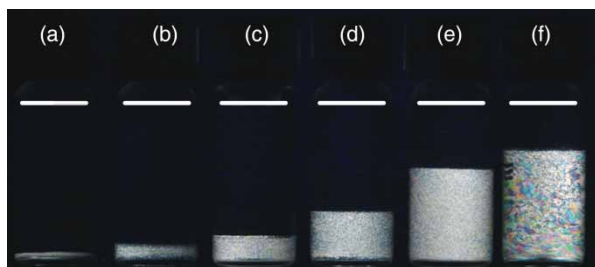


Figure 5. Aqueous suspensions of beidellite at an ionic strength of 10^{-4} M observed between crossed polarizer and analyzer. (a) $\phi = 0.40\%$; (b) $\phi = 0.42\%$; (c) $\phi = 0.44\%$; (d) $\phi = 0.46\%$; (e) $\phi = 0.48\%$; and (f) $\phi = 0.50\%$. (The white bars indicate the level of suspension in the vials.)

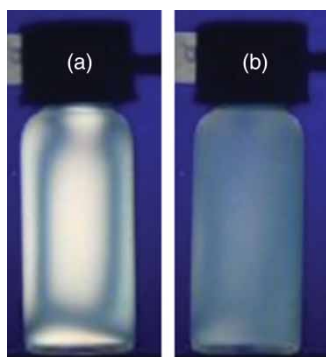


Figure 6. Aqueous suspension of beidellite (ionic strength: 10^{-3} M, $\phi = 0.43\%$) showing (a) flow birefringence (photograph taken right after flow) and (b) relaxation after the flow.

transition and X-ray scattering shows (see next section) that this liquid-crystalline phase is actually nematic. Note that, to the best of our knowledge, Langmuir was the first scientist to report the existence of the nematic phase in clay suspensions.[24] However, he also reported in the same article that this observation was not reproducible. It actually took decades to realize that proper control of clay nature, purity, and polydispersity, and of the suspension ionic strength are required to achieve the reproducibility of these subtle phenomena.[44]

As expected, more dilute samples are fully isotropic, whereas more concentrated ones are entirely birefringent. However, the isotropic phase has strong flow birefringence, which means that it still contains a significant amount of suspended clay sheets (Figure 6). Aqueous suspensions of synthetic clays, like sodium fluorohectorite, also revealed comparable birefringence properties.[46]

The observation by polarized-light microscopy of biphasic samples held in flat glass capillaries reveals (Figure 7) the presence of small birefringent nematic droplets (often called tactoids in the literature) floating in the isotropic liquid, which is very classical for similar lyotropic systems.[47] Typically, these tactoids appear on a time scale of a few days and the phase separation is completed, under

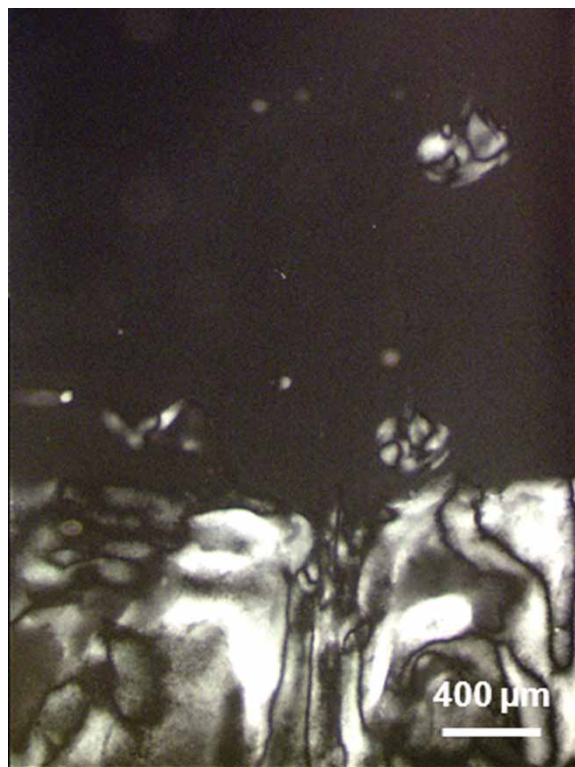


Figure 7. Formation and sedimentation of nematic droplets (tactoids) in aqueous suspensions of beidellite ($\phi = 0.50\%$) at an ionic strength of 10^{-4} M, observed by polarized-light microscopy ($0.2 \text{ mm} \times 2 \text{ mm}$ flat capillary).

the influence of gravity, in a few weeks. Then, polarized-light microscopy often reveals the Schlieren textures of a nematic phase.[48]

An example of phase diagram of such systems, as a function of volume fraction and ionic strength, is shown in Figure 8.[41] For this particular type of clay, it appears that the I/N transition occurs at volume fractions slightly lower than the sol-gel transition. Therefore, the phase diagram displays a narrow region of fluid nematic phase. Upon increasing ionic strength, the tilt of the phase boundaries towards larger volume fractions shows that both the gel state and the fluid nematic phase are slightly destabilized with respect to the isotropic phase until flocculation of the system occurs at ionic strengths around 5×10^{-3} M. Moreover, no significant influence of temperature on the phase diagram was detected, up to 100°C . This observation suggests that this I/N transition may be explained by the Onsager model or by numerical simulations of plates only interacting through hard-particle repulsions.[1,49–51]

Indeed, numerical simulations of polydisperse, hard and thin, platelets predict the coexistence of nematic and isotropic phases at numerical densities, n_I and n_N , given by: $n_I \langle D^3 \rangle \sim 3.7$ and $n_N \langle D^3 \rangle \sim 4.0$ (where the brackets mean an ensemble average), which can be converted into the volume fractions of the coexisting phases (ϕ_I and ϕ_N),

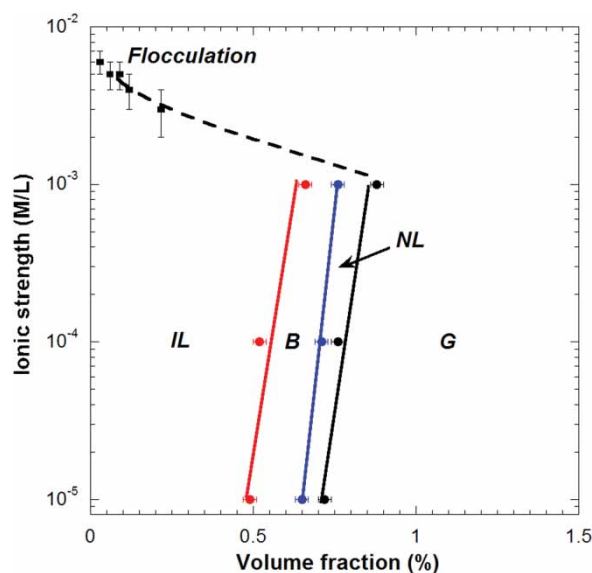


Figure 8. Typical phase diagram obtained for the size-selected aqueous beidellite suspensions (Size 2).

Note: IL, isotropic liquid; B, biphasic liquid; NL, nematic liquid; and G, gel.

using the particle volume $\pi/4(D^2t)$. For example, the phase diagram of the beidellite clay shown in Figure 8 gives $\phi_I \sim 0.5\%$ and $\phi_N \sim 0.7\%$ compared with predicted values of 0.8% and 0.9% , respectively. Thus, semi-quantitative agreement is obtained between experimental observations of the nematic ordering and numerical simulations. Still, electrostatic repulsions should also be taken into account in order to reach a better description of these charged particles in water. This is, however, a very challenging task that is only presently being tackled.[52,53]

In contrast with other model systems, the phase diagram of aqueous clay suspensions did not reveal so far any other type of liquid–crystalline phase, such as lamellar or columnar mesophases.[54,55] The formation of the latter implies the appearance of well-defined periods, which may be hindered by the large polydispersity of the clay platelets.

The topology of the phase diagram of aqueous clay suspensions is very different from that of other suspensions of nanosheets that display a lamellar mesophase.[55] In that case, the lamellar phase can usually be swollen until some limit is reached. Then, excess solvent is expelled but, at any further dilution, some lamellar phase remains, in contrast with the nematic phase of clays that completely disappears below ϕ_I .

The phase diagram of bentonite (Figure 9) does not display a fluid nematic phase.[56] Instead, birefringent gels are observed and even though these gels show typical nematic textures, they do not align in electric or magnetic fields. Therefore, a direct transition from the isotropic liquid to an arrested state occurs, as if the I/N phase transition were pre-empted by the sol–gel transition. A similar phase diagram

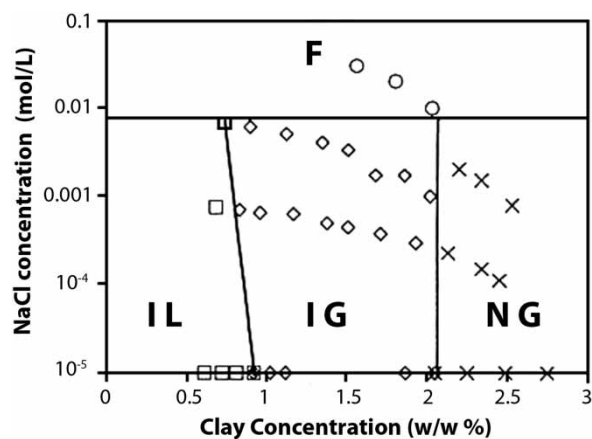


Figure 9. Phase diagram of Laponite suspensions versus clay and NaCl concentrations.

Note: F, Flocculated samples; IL, isotropic liquid; IG, isotropic gel; and NG, nematic gel.

is also observed for the aqueous suspensions of synthetic Laponite clay that is very popular for soft condensed matter studies because it is commercially available.[56]

4. Structural studies of clay suspensions

The mesophases detected by optical observations in colloidal suspensions of clay nanosheets can be studied in more detail by X-ray scattering. Indeed, thanks to the good electronic contrast between the nanosheets and the solvent, the structure of the suspensions can be easily studied by this technique, in spite of the low volume fractions of the samples. Because of the large size of the platelets (100–500 nm), the relevant X-ray scattering signal lies at small scattering angles. Moreover, because of the large dilution, the typical distance between the platelets ranges from 10 to 100 nm. Such large distances and, therefore, low scattering angles can be probed by small-angle X-ray scattering (SAXS) available worldwide at most synchrotron radiation facilities.

Very dilute ($\phi < 0.1\%$) colloidal suspensions of clay nanosheets can be examined by SAXS in order to obtain the particle form factor. Indeed, at such dilutions, all positional and orientational correlations between platelets can be neglected. The dependence of the scattered intensity, I , versus scattering vector modulus q ($q = (4\pi/\lambda) \sin \theta$), where λ is the wavelength and 2θ the scattering angle) follows a $I \sim q^{-2}$ decay law in the range $2\pi/D < q < 2\pi/t$ (Figure 10). This dependence is typical of well-dispersed two-dimensional objects.

Structural studies of the nematic phase are most conveniently performed when single domains are available. We will show in the next section how such single domains can be produced. The SAXS pattern of an aligned nematic sample of beidellite clay suspension (Figure 11) is highly anisotropic but only displays a row of equidistant diffuse

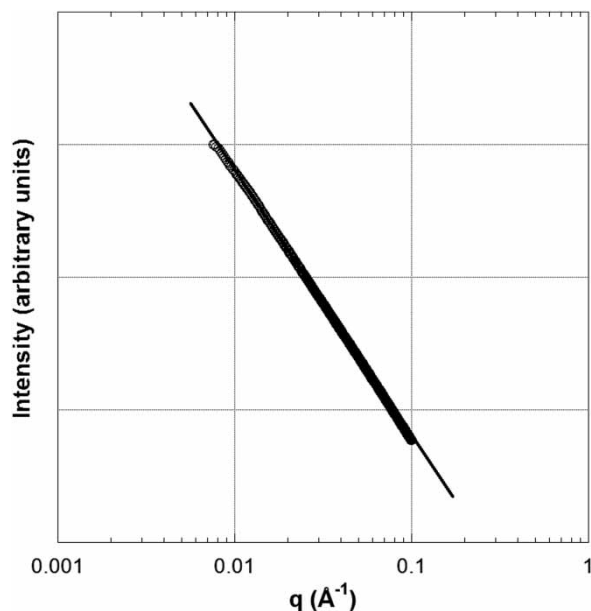


Figure 10. Variation, in log–log representation, of the scattered intensity as a function of q for a size 3 beidellite suspension in the dilute regime.

Note: The solid straight line, with a slope of -2 , is a guide to the eye whereas the open circles are the experimental data points.

spots in a direction parallel to the director. The absence of any sharp diffraction lines or spots proves that the nanoparticles have no long-range positional order. The SAXS pattern is, therefore, typical of a nematic phase. The diffuse spots arise from a local, liquid-like, one-dimensional positional order of the clay platelets. This stacking period is close to 50 nm, which is about two orders of magnitude larger than the 0.7 nm thickness of the nanosheets. This is of course related to the very low volume fractions ($\phi \sim 1\%$) of these suspensions. It is interesting to examine the swelling law – i.e. the way in which the average distance, d , between platelets varies with the volume fraction (Figure 12).[57]

In the nematic state (i.e. both in the fluid nematic phase and in the birefringent arrested state), a $d = \delta \cdot \phi^{-1}$ dependence is observed, which is usually characteristic of a lamellar order, like in a L_α phase of surfactants. The value of δ is usually very close to the nanosheet thickness when clay exfoliation has been properly performed. A significantly larger value of δ means that an appreciable fraction of clay nanosheets are still stuck together in pairs or even in small stacks. This provides a very convenient and stringent test of the good dispersion of the clay platelets.

In the isotropic phase but close to the nematic phase ($0.1\% < \phi < 0.5\%$), the SAXS patterns remain isotropic in the absence of external field (like flow or electric field) but show diffuse rings that modulate the q^{-2} intensity decay. This means that positional correlations between platelets may no longer be neglected. In other words, the scattering now results not only from the particle form factor but

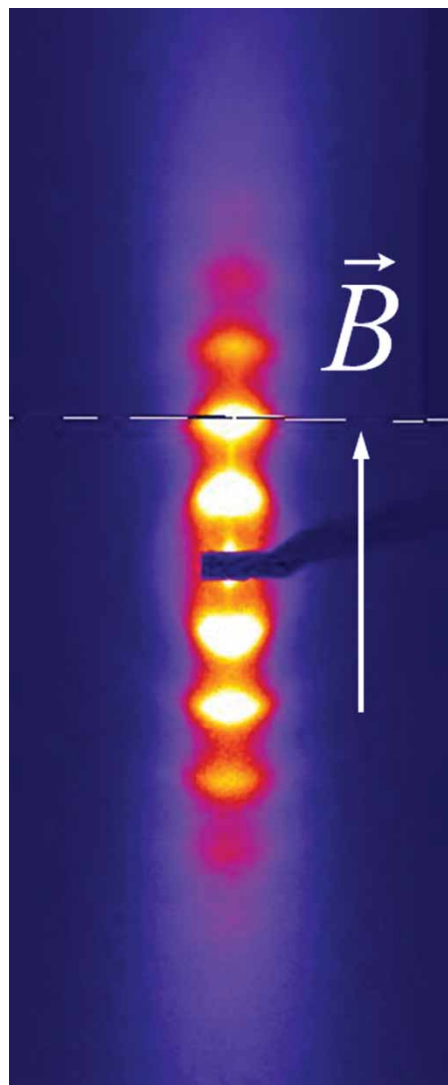


Figure 11. SAXS pattern of size 3 beidellite suspension ($\phi = 0.52\%$, ionic strength: 10^{-4} M) previously submitted to a vertical $B = 8$ T magnetic field.

also from the suspension structure factor. In this regime, the change with volume fraction of the position of the first scattering ring can also be represented (Figure 12). One notices a crossover from the $\sim \phi^{-1}$ dependence to a $\sim \phi^{-1/3}$ dependence, more typical of the homogeneous swelling of spheres, which suggests that orientational correlations between platelets are lost at volume fractions below $\phi \sim 0.5\%$, i.e. around the I/N transition. Note that this reasoning remains very qualitative due to the absence to date of any rigorous treatment of the SAXS signals from anisotropic objects that have coupled orientational and translational correlations.

The anisotropy of the SAXS pattern of a single domain of the nematic phase can be modelled to derive the nematic order parameter, S . The simplest procedure consists in recording the SAXS intensity scattered along a circle going through the first diffuse spot versus azimuthal angle φ

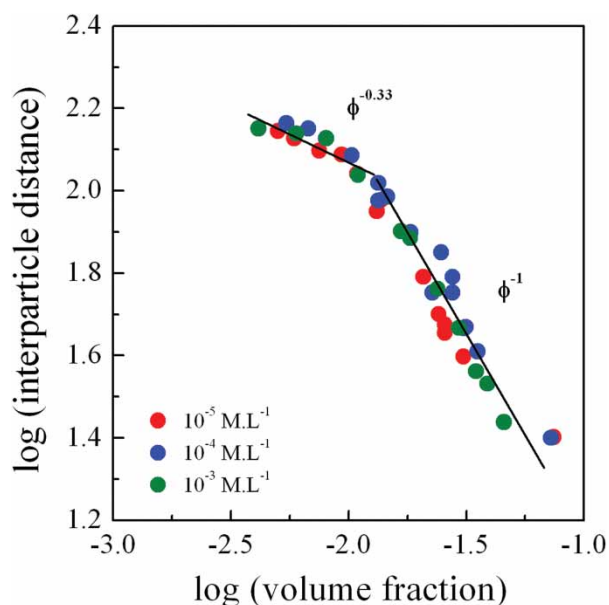


Figure 12. Variation of the average interparticle distance with volume fraction at different ionic strengths for size 1 beidellite suspensions.

Note: Distances are reported in nanometers.

(Figure 13). The case of clay nanosheets is particularly simple for this purpose because their diameter is much larger than their average distance and thickness. Because the diffuse spot arises from stacking positional correlations, the intensity scattered (properly corrected for background and all other classical corrections) at an angle φ is directly proportional to the fraction of particles whose normals lie at the same angle φ with respect to the director \mathbf{n} . This fraction is given by the orientational distribution function (ODF) of the nematic phase, whose second-order moment is S .^[58] The nematic phase of clay nanosheets is actually one of the few cases where assimilating $I(\varphi)$ to the ODF is a good approximation. Then, for the ODF, one may use the classical Maier–Saupe distribution function in order to fit the data (Figure 13) and calculate S . Very large values of S , $S \sim 0.8$, are thus obtained, in good agreement with the strongly first-order character of the I/N transition predicted for these suspensions.

Although quite prominent on the SAXS patterns, the diffuse spots due to platelet local stacking still remain fairly broad. In spite of the existence of harmonics, the breadth of the scattering spots shows that the mesophase is indeed nematic rather than lamellar, in agreement with the topology of the phase diagram. For comparison, the SAXS patterns of other colloidal suspensions of synthetic nanosheets display much sharper diffraction features that, in some cases, could even be properly analysed in the usual framework of lamellar phases (lineshape analysis using the Caillé formalism).^[59]

Wide-angle X-ray scattering can also bring valuable structural information about colloidal clay suspensions.

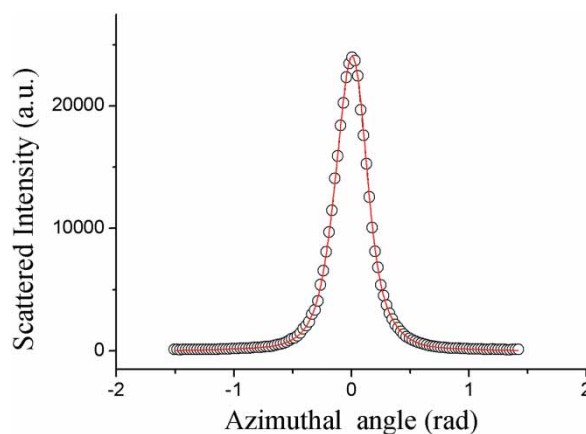


Figure 13. ODF derived from the SAXS pattern of a beidellite suspension aligned in a magnetic field.

Note: The solid line is a fit used to calculate the moments of the distribution, including S .

Indeed, the atomic crystalline order that prevails within each nanosheet gives rise to thin diffraction lines corresponding to typical inter-atomic distances. For example, a sharp peak is observed at $q \sim 14 \text{ nm}^{-1}$ and corresponds to the $d(20-; 11-)$ reflection of the clay sheet structure. Note that the nematic order parameter of an aligned nematic sample can also be estimated from the azimuthal profile of this wide-angle reflection.^[60,61]

5. Anchoring of the nematic phase

One of the distinctive properties of liquid–crystalline phases is the spontaneous “anchoring” of the director on surfaces, i.e. the well-defined orientation of the director at a surface and the propagation of this director orientation from that surface into the bulk material. When filled into optical flat glass capillary tubes, as observed for gibbsite platelet suspensions,^[62] the nematic phase of clay suspensions often strikingly displays homeotropic anchoring, with the nematic director perpendicular to the glass surface. Figure 14 shows a biphasic I/N sample in an untreated flat glass capillary observed between crossed polarizers. The upper part of the sample is isotropic and, therefore, appears completely dark, as expected. However, the lower part of the sample that is nematic also appears dark between crossed polarizers. The boundary between the two phases is, therefore, barely visible. The reason why the nematic phase appears dark is that it is homeotropically anchored onto the glass surface.^[63] Because the nematic director (i.e. the phase symmetry axis) is parallel to the light beam, no birefringence can be detected. Indeed, the nematic phase shows thin bright regions at the sides of the capillary due to homeotropic anchoring on the side walls.

By shining an X-ray beam on this homeotropic nematic sample, parallel to the glass plates rather than along their normal, a quite anisotropic SAXS pattern can be recorded

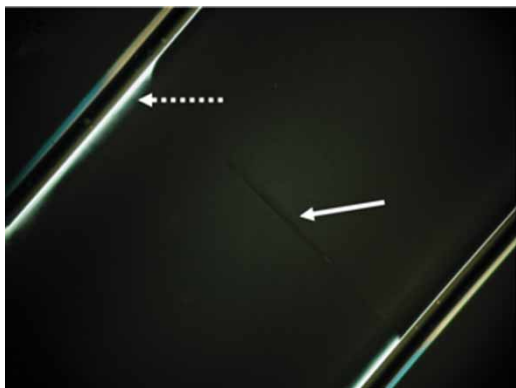


Figure 14. Polarized-light microscopy image of a biphasic sample of a beidellite suspension (ionic strength: 10^{-4} M, $\phi = 0.57\%$) in a flat glass capillary (2 mm wide).

Note: The white arrow points to the (barely visible) meniscus between the isotropic phase in the upper right part and the nematic phase in the bottom left part. The nematic phase is in the homeotropic orientation due to wall-anchoring and therefore appears as dark as the isotropic phase. The broken white arrow points to a bright area at the edge of the nematic phase where the anchoring is planar due to the influence of the side walls of the capillary.

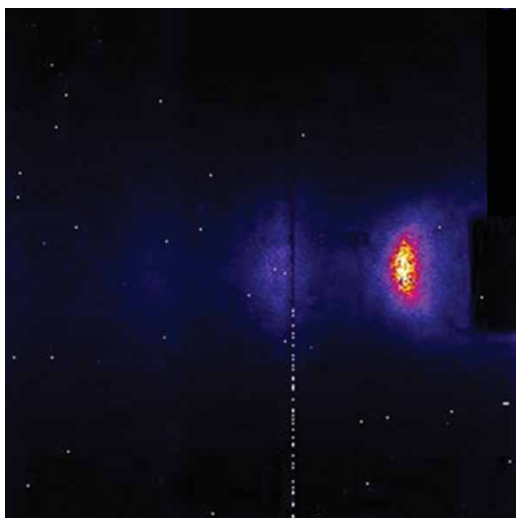


Figure 15. SAXS pattern of a homeotropic nematic sample of beidellite suspension (ionic strength: 10^{-4} M; $\phi = 0.62\%$).

(Figure 15) that is similar to the one shown in the previous section (Figure 11).

These experimental observations precisely agree with the theoretical predictions of homeotropic anchoring of a nematic suspension of hard platelets at a wall.[64] In contrast, planar anchoring is expected for a nematic suspension of hard rods. It should be noted that in the nematic phase of colloidal suspensions, the anchoring is mostly of entropic origin, i.e. it is mainly due to excluded volume effects between the particles and the cell wall. However, in usual thermotropic liquid crystals, the anchoring energy is mostly of enthalpic origin, i.e. it is due to the interaction energy of

the liquid-crystal molecules with the wall. Strictly speaking, the entropic anchoring energy is not a surface energy, but only a surface-like contribution, as it also depends on the bulk properties and not only on the interactions close to the surface. In fact, if the cell thickness d is smaller than the largest dimension L of the particle, the anchoring strength becomes infinite, as the orientation of the platelet perpendicular to the wall is physically impossible. However, if $d \gg L$, the anchoring becomes rather weak, due to the relatively small entropy gain when L is parallel to the wall. Similarly, the well-known Berreman's contribution to the anchoring energy of thermotropic liquid crystals is also a surface-like term, arising from the integration of the bulk elastic energy, and not from the molecule-wall interaction energy.[58]

6. Influence of magnetic and electric fields

Another distinctive property of liquid-crystalline phases is their ability to respond to an external field, so that they can be considered as “soft” condensed matter. As described above, the phase diagrams of aqueous suspensions of some natural clays display a thin region where the nematic phase is stable. In this region, magnetic- and electric-field alignment properties are expected, as observed with usual thermotropic liquid crystals. Due to the small volume fraction and the weak contrast in magnetic permeability between the clay nanosheets and the solvent, in spite of the huge aspect ratio of the particles, the anisotropy of magnetic susceptibility of the nematic phase remains rather small. Therefore, large magnetic fields of the order of several Teslas must be applied in order to turn a “powder-like” distribution of nematic domains into a single domain. A notable exception is that of nontronite clay that contains significant amounts of iron (III) in its chemical composition.[44] Indeed, nontronite nematic suspensions completely align in the 1T field produced by small NdFeB permanent magnets (Figure 16). Interestingly, the isotropic phase also becomes birefringent when submitted to the magnetic field. Such magnetic-field-induced orientational order was already reported for the isotropic suspensions of gibbsite platelets but at much higher concentration and field intensity. In nontronite suspensions, the strength of this effect hints at peculiar magnetic properties of the nontronite nanosheets.

A sudden change of direction of the magnetic field brings about a transient hydrodynamic instability due to the reorientation of the nematic director, which gives rise to a striped texture (Figure 17). Such instability is actually classical and was first observed in suspensions of the Tobacco Mosaic Virus [65] and more recently in suspensions of gibbsite platelets.[62,66–69] The modulation period can be adjusted by varying the field intensity or the sample thickness and the transient state could be frozen-in by UV-polymerization of a water-soluble monomer, as described later in this article.

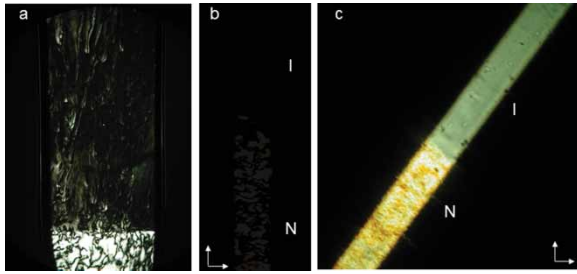


Figure 16. (a) Polarized-light optical microscopy observations of a nontronite suspension ($\phi = 0.7\%$, ionic strength: 10^{-3} M) at the onset of phase separation. (b) and (c) Polarized-light optical microscopy observations of a biphasic sample of a nontronite suspension ($\phi = 0.7\%$, ionic strength 10^{-3} M) held in a flat capillary submitted to a horizontal $1-T$ magnetic field.

Note: White arrows indicate the directions of the polarizers. *I*, isotropic phase; *N*, nematic phase. (b) Extinction conditions. The capillary is barely visible because its axis is parallel to that of the polarizer. (c) Maximum transmission conditions. The nematic phase is almost uniformly bright because there are only very few defects left. The isotropic phase is not dark because of its large magnetic-field-induced anisotropy.

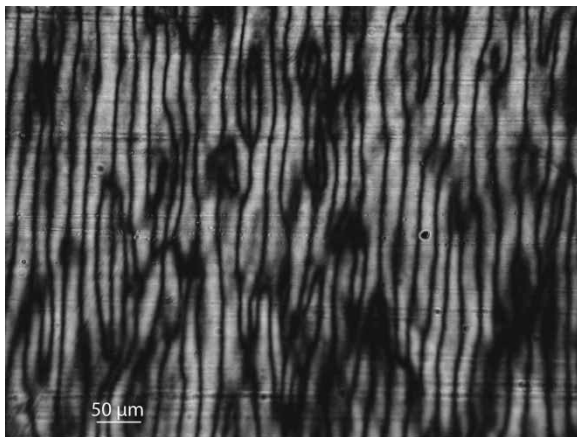


Figure 17. Transient hydrodynamic instability observed upon a sudden change of 90° of the magnetic field direction for a nontronite suspension ($\phi = 0.7\%$, ionic strength: 10^{-3} M) held in a flat glass capillary.

A detailed polarized-light microscopy and SAXS investigation of the magnetic-field alignment of beidellite suspensions has shown that beidellite platelets orient their normal parallel to the magnetic field. This means that the anisotropy $\Delta\chi_m = \chi_{//} - \chi_{\perp}$ of magnetic susceptibility is positive ($\chi_{//}$ and χ_{\perp} represent the magnetic susceptibility parallel and perpendicular to the director, respectively). Moreover, the production of this aligned domain allowed measuring the birefringence $\Delta n = n_e - n_o = -(4.1 \pm 0.3) \times 10^{-4}$, which is negative and has a value typical for such dilute suspensions of highly anisotropic objects (n_e and n_o represent the optical indices of the nematic phase parallel and perpendicular to the director, respectively). The phase birefringence is given by:

$\Delta n = \Delta n_{\text{sat}} \phi S$, where Δn_{sat} is the specific birefringence of the nanoparticle.

An investigation of organically modified montmorillonite platelets has shown that these nanosheets align parallel to the field when suspended in dodecanol, but they align their normal parallel to the field when dispersed in small amounts in the nematic phase of 5CB. This was explained by the homeotropic anchoring of 5CB on the clay platelets.[70]

The application of electric fields onto colloidal aqueous suspensions requires particular caution because of the large sample conductivity due to the presence of ions. In order to avoid the screening of the electric field, high-frequency a.c. voltages must be applied to the samples.[71] More precisely, the frequency must be higher than $K_e/(2\pi\epsilon_0\epsilon_e)$ where K_e is the conductivity of the suspension, ϵ_0 the electric permittivity of vacuum and ϵ_e the dielectric constant of the suspension. In practice, a frequency of ~ 500 kHz was used in the experiments with clay suspensions. Moreover, the electric field was applied to the sample, held in a glass capillary, using a pair of external ring-shaped electrodes, which avoids charge injection and easily allows moving the sample in the field and even changing samples rapidly. With this kind of setup, the effect of the field on the sample could be followed *in situ* and in real time by monitoring its birefringence or by recording its SAXS patterns. More experimental details on this setup are given in reference [71] and similar experiments were also performed with aqueous suspensions of niobate nanosheets.[72]

Observations with polarized-light microscopy demonstrate that the nematic phase of beidellite suspensions is easily aligned by the a.c. electric field (Figure 18). However, the anisotropy of the dielectric constant, $\Delta\epsilon = \epsilon_{//} - \epsilon_{\perp}$, being negative, the nematic director aligns in a plane perpendicular to the field, resulting in a two-dimensional distribution of nematic domains. This means that the nanosheets align with their normal perpendicular to the electric field. Sometimes, one of these domains grows at the expense of the others and a single nematic domain, large enough for SAXS studies, can be obtained (Figure 19). (Note that the symmetry of the sample is then biaxial since the uniaxial symmetry is

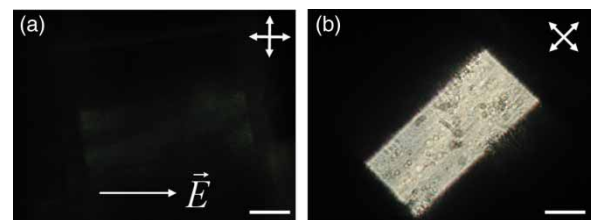


Figure 18. Optical textures in polarized-light microscopy of a fluid nematic sample of beidellite suspension (ionic strength: 10^{-5} M and $\phi = 0.61\%$) in a 1 mm cylindrical glass capillary aligned in a 4×10^4 V/m, 500 kHz electric field at (a) 0° and (b) 45° with respect to the crossed polarizers (white arrows); scale bar : 500 μm .

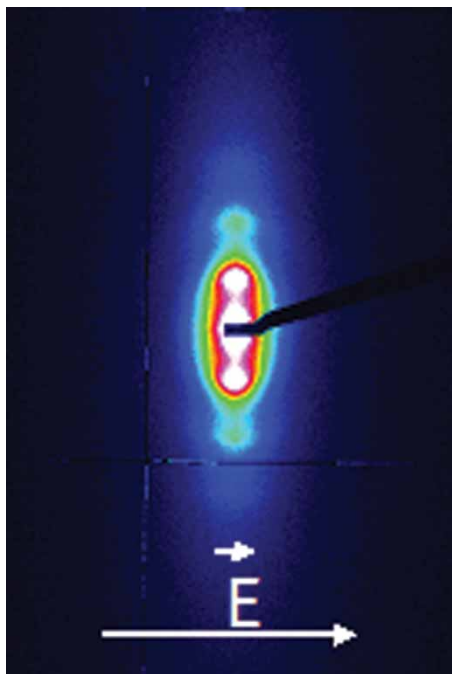


Figure 19. SAXS pattern of a nematic beidellite suspension (ionic strength: 10^{-4} M; $\phi = 0.52\%$) in a 1 mm cylindrical glass capillary aligned in a 4×10^4 V/m, 700 kHz horizontal electric field.

broken by the field that is perpendicular to the director \mathbf{n} .) The nematic order parameter, $S \sim 0.8$, of this sample can be deduced from the measurement of its birefringence. The most important effect of the field is to change the direction of \mathbf{n} without significantly altering the value of S .

The isotropic phase shows a very different scenario upon application of the electric field. Figure 20 shows an isotropic sample of clay suspension submitted to an a.c. electric field and in the absence of field, observed by polarized-light microscopy. This sample, isotropic in zero-field, becomes quite birefringent when submitted to the field. This birefringence (Figure 21) can be used to calculate the field-induced orientational order, S_i , as a function of field intensity. At low fields, as expected, S_i follows a quadratic dependence on field intensity but a crossover soon appears and the field-induced order saturates at high field. The analysis of the birefringence then shows that all the nanosheets are aligned with their normal perpendicular to the field direction but the phase keeps uniaxial symmetry. The maximum saturated value of the field-induced orientational order is therefore $S_i = -1/2$ and this kind of orientational order is sometimes called “antinematic”. In the dilute regime, the field-induced birefringence at saturation is proportional to the particle volume fraction and this law holds until the biphasic region is reached.

The technical complications involved in electro-optic studies of aqueous colloidal clay suspensions can sometimes be avoided by grafting organic molecules at the surface of the clay nanoparticles in order to suspend them in

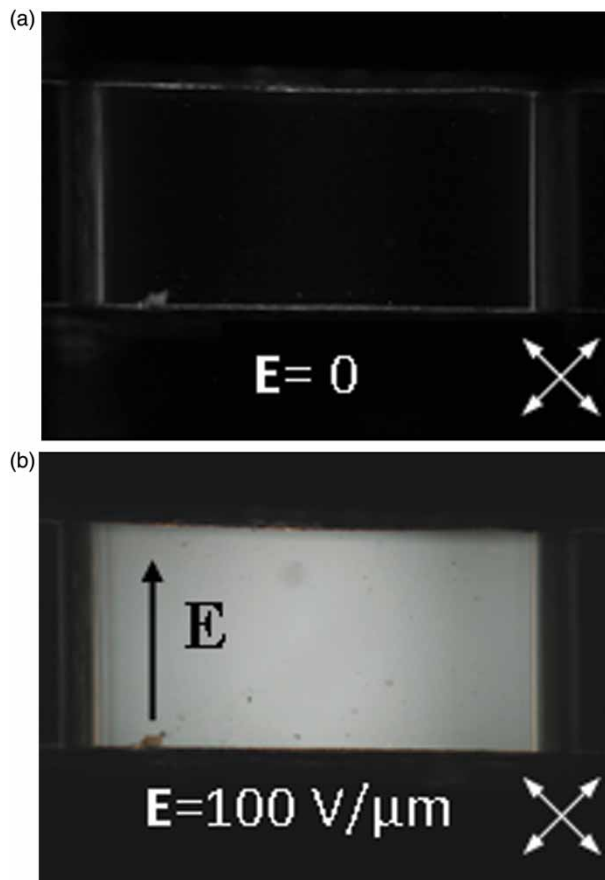


Figure 20. Electric birefringence in the isotropic phase of a beidellite clay suspension ($\phi = 4.1 \times 10^{-3}$). Microphotographs of the sample between crossed polarizers (the white arrows at 45° to the field direction) before (a) and after (b) the application of the field ($\nu = 500$ kHz, amplitude of the applied voltage $U_0 = 140$ V).

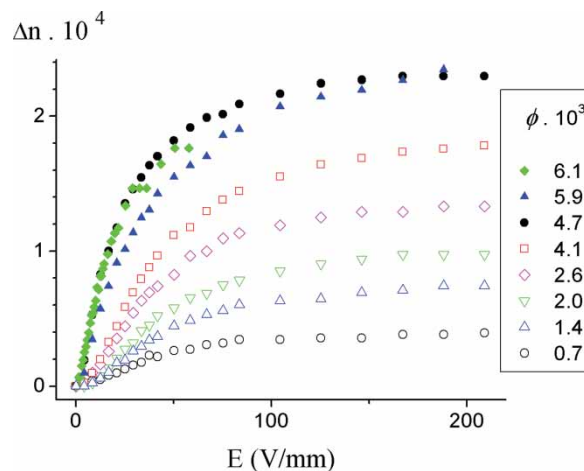


Figure 21. Evolution with ϕ of the electric birefringence in the isotropic phase of a beidellite clay suspension.

an organic solvent. For example, the suspensions of sodium fluorohectorite platelets in silicone oil displayed interesting electric-field-induced alignment properties.[73]

7. Flow properties

For industrial applications, aqueous suspensions of natural clays are most often used as additives to adjust the viscoelasticity of complex fluids such as oil-drilling muds for instance. The flow properties of clay colloids are quite complicated and have been studied for decades with only limited progress in their understanding so far. The underlying reason for that probably lies in the difficulty of modelling the electrostatic interactions of anisotropic charged particles in aqueous solvents. In practice, the behaviour of clay colloids under flow displays two striking phenomena.

Firstly, as mentioned before, for concentrations larger than that of the sol–gel transition, a yield-stress is observed below which the colloidal suspension does not flow (Figure 22). The yield-stress depends on the clay volume fraction. This feature does not seem to be related to the possible existence of any liquid–crystalline order since there are clay gels, like some Laponite gels (in a given range of volume fraction), that show a yield-stress but no birefringence.

Secondly, clay sols (i.e. clay suspensions of volume fractions lower than that of the sol–gel transition) are strongly shear-thinning fluids (Figure 22). This is quite expected from a nematic material. Indeed, in the typical way in which these rheology experiments are performed, no particular attention is paid to texture control. Therefore, at the start of the experiment, the sample is either not aligned at all and has many topological defects or is aligned in some more or less random direction. In any case, as the sample starts flowing,

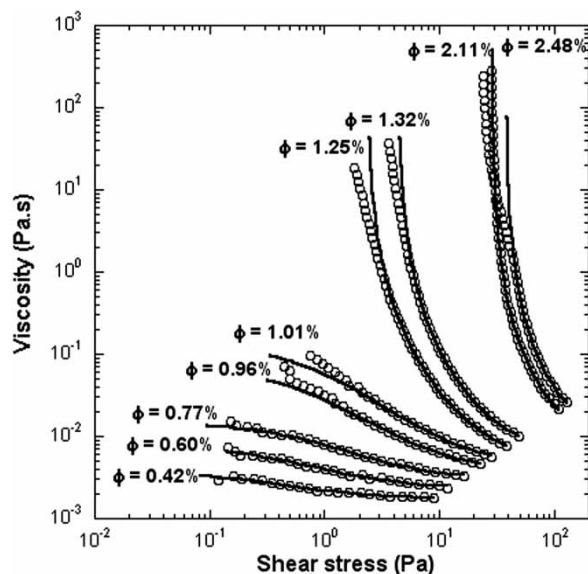


Figure 22. Typical shear-thinning behaviour observed in flow curves (viscosity vs shear stress) for beidellite suspensions (size 1, ionic strength: 10^{-5} M). The onset of a yield-stress appears in this experiment as a change in the concavity of the flow curves between $\phi = 1.01$ and 1.25% .

Note: Open circles: experimental curve. Solid black line: modelled curve.

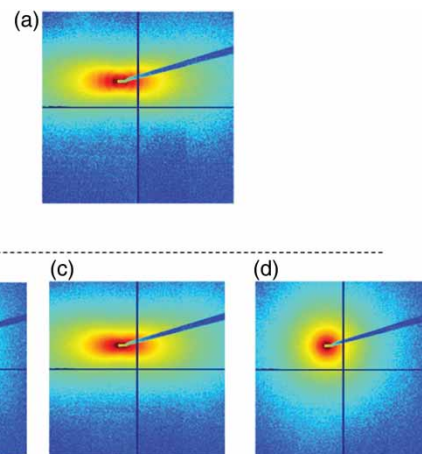


Figure 23. SAXS patterns measured during shear-flow experiments for two different suspensions of Beidellite (size 2, ionic strength: 10^{-4} M).

Note: a: nematic sample ($\phi = 0.66\%$) sheared at 50 s^{-1} ; b, c, and d: isotropic liquid ($\phi = 0.42\%$) before shearing, sheared at 1000 s^{-1} , and after shearing, respectively. In the SAXS pattern reference frame, the horizontal and vertical directions correspond respectively to the velocity gradient and the vorticity directions.

in order to minimize dissipation, the nematic phase aligns with respect to the flow direction, revealing its lowest viscosity. This orientation process can easily be monitored by *in situ* SAXS using a Couette shear cell, especially adapted to X-ray scattering, which allows the diffraction pattern to be recorded whilst the sample is being sheared between two concentric cylinders. As intuitively expected, at high shear rates, the clay platelets align parallel to the shearing surfaces, i.e. with the nematic director parallel to the velocity gradient (Figure 23(a)). Interestingly, this behaviour is also commonly observed for the flow of lyotropic lamellar phases of surfactants.[74]

Shear-thinning is in no way restricted to the nematic phase of clay suspensions and it is actually also ubiquitous in the isotropic phase at all concentrations (Figure 23(b)–(d)). Flow alignment effects were predicted and even calculated for a single platelet and must be considered both in shear and elongational hydrodynamic flows. Further complications also arise due to multiple hydrodynamic interactions and to the electrostatic repulsions between the charged platelets. However, a simple approach, mostly based on excluded volume effects, gives a reasonable semi-quantitative description of the shear-thinning behaviour.[75,76]

Both theoretical and experimental studies of the flow properties of lyotropic nematic suspensions of rod-like particles are rather scarce. The situation is actually much worse for nematic suspensions of plate-like particles. For example, the anisotropy of the viscosity and its dependence on platelet concentration and size remain largely unknown. Experimental investigations and numerical simulations in well-defined geometries are badly needed to make progress in this rather new field.

8. Applications and perspectives

In terms of applications, the orientational order of nanosheets in suspension, either spontaneous or field-induced, is already exploited in many cases, such as in gas-barrier clay-plastic hybrids.[77] Furthermore, many industrial uses of clays, like in drilling muds or paints, are based on their viscosity-modifying properties that are related to clay platelet alignment. However, more recent applications that specifically exploit the properties discussed in this article were recently described in literature.

In a first example, composite clay/polymer materials were prepared in which the clay platelets are aligned in an electric field.[78] A hydrosoluble acrylamide monomer was added to an aqueous suspension of clay nanosheets, together with N,N' -methylenebisacrylamide, riboflavin, and N,N,N',N' -tetramethylethylenediamine, used respectively as cross-linker, initiator, and catalyser. Luckily, this mixture still showed the liquid-crystalline nematic phase and its field-alignment properties. However, simple experiments were carried out in the isotropic phase because it does not require any texture control. Acrylamide polymerization can be performed by heating the sample or, more conveniently, under irradiation with UV-light. Thus, self-standing nanocomposite clay/polyacrylamide hydrogels of mm to cm size were easily obtained. Polymerization can even be triggered *in situ* by the light source of a usual optical microscope while the electric field is applied to the sample. Another advantage of the isotropic phase over the nematic one for this purpose is that the magnitude of its orientational order can be easily controlled and adjusted by varying the intensity of the applied a.c. electric field (as described above) while polymerization proceeds (Figure 24). Antinematic order of variable strength can, therefore, be frozen-in within colloids of clay nanosheets.

Moreover, because the polymerization reaction takes minutes and the diffusion constants of the reagents are not too large, modulating in time the applied electric field, using square signals can even be worthwhile. Indeed, if UV-light is then shone only at one side of the sample, a polymerization front appears that travels through the sample to its other side. When the electric field is on, the polymerization front freezes a region that shows field-induced orientational order whereas when the field is off, it freezes an isotropic region. In polarized-light microscopy, this results in a striped texture due to the alternation of aligned and isotropic regions, with a modulation period that can easily be tuned between about 20 μm and 1 mm (Figure 25). In this way, birefringent gratings can be produced in a very cheap and simple fashion. Note that several other examples of clay/polymer composites with clay nanosheets aligned in external fields were also reported in the literature.[79,80]

Inorganic-inorganic hybrid composite materials based on clays might also be produced like those based on the nematic phase of V_2O_5 nanoribbons.[81] In that case, single-domain mesostructured silica/ V_2O_5 composites of

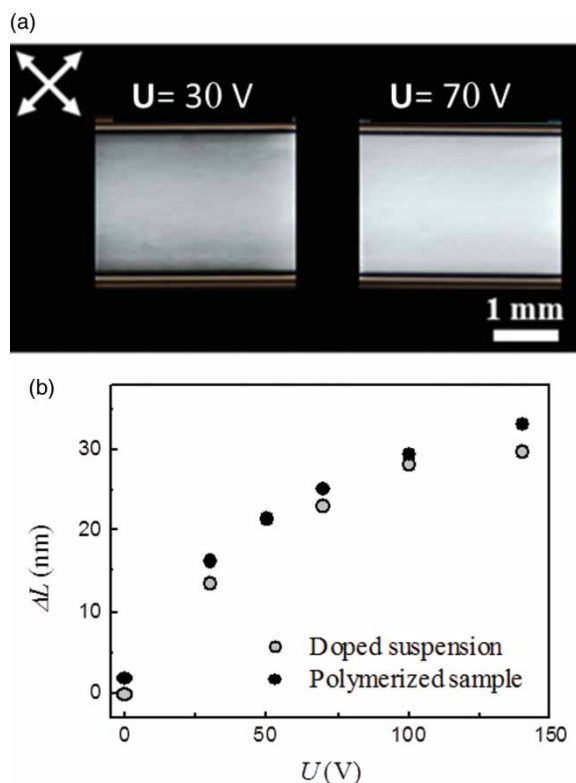


Figure 24. (a) Polarized-light optical microscopy images between crossed polarizers (white arrows) of the field-induced birefringence of samples polymerized at different voltages; (b) phase-shift measures before (gray) and after (black) polymerization, as a function of the voltage applied during polymerization. (The clay volume fraction is $\phi = 0.4\%$.)

centimetre size were produced in a small magnetic field. Furthermore, the V_2O_5 template could be leached out of the silica matrix, leaving aligned and empty channels. Hence, large colourless, transparent, and birefringent mesoporous monoliths were obtained with a high specific surface area suitable for catalytic applications.

From another perspective, the orientational order induced by an a.c. electric field in isotropic suspensions of clay nanosheets may also find applications in electro-optic devices. Indeed, the use of the isotropic phase instead of usual thermotropic nematic phases dispenses with the need of controlling the texture. Moreover, such aqueous suspensions of natural clays may be more environment-friendly and less expensive than common small-molecule liquid-crystals.

Liquid-crystalline colloids of synthetic nanosheets have also found an application in a rather unexpected field. Indeed, the lamellar phase of the aqueous suspensions of $\text{H}_3\text{Sb}_3\text{P}_2\text{O}_{14}$ nanosheets aligned in a magnetic field were used to measure by nuclear magnetic resonance the residual dipolar couplings of dissolved biomolecules such as polypeptides or sugars.[55] This technique allows determining the conformation of nonlabelled biomolecules accurately. Compared to other complex fluids, such as surfactant

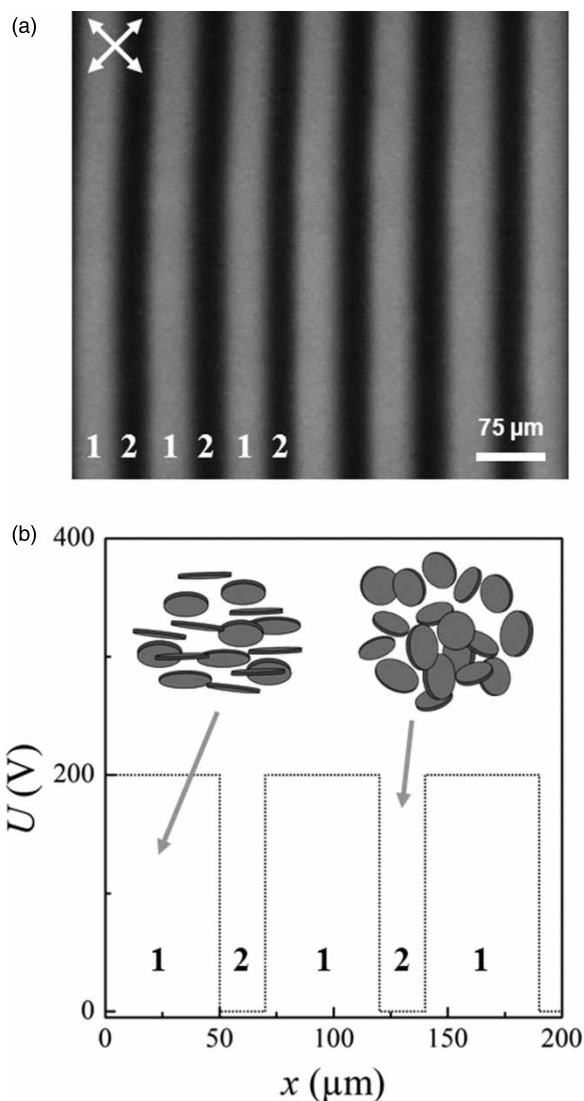


Figure 25. (a) Polarized-light optical microscopy image between crossed polarizers (white arrows) of a composite sample ($\phi = 0.4\%$) patterned with a step-like modulation. (b) Corresponding applied a.c. voltage amplitude at the position of the travelling polymerization front. The sketches represent either the (1) antinematic or (2) isotropic platelet organization.

solutions and virus suspensions, used for the same purpose, mineral nanosheet colloids have the following advantages: (i) the liquid-crystalline phase occurs at much lower colloid volume fraction; (ii) some of these systems, when prepared in D_2O , have no hydrogen, carbon, or nitrogen atoms, which dispenses from the need of biomolecule selective isotope labelling; (iii) usually, nanosheet suspensions are very stable in time and in the temperature range ($4\text{--}50^\circ\text{C}$) useful for biomolecules; and (iv) the biomolecules can be easily recovered by flocculation of the nanosheets.

A last example of applications deals with aqueous colloidal mixtures of natural clay and synthetic niobate nanosheets.[82,83] The semiconducting nature of niobates makes them interesting materials for use in photoelectric

devices. When cationic electron acceptor methyl viologen molecules are added to the colloidal mixtures, they selectively adsorb onto the clay nanosheets. Even though these systems are homogeneous on a macroscopic scale, the clay and niobate nanosheets tend to segregate at the microscopic scale. The niobate particles are photoactive electron donors so that, due to the large distance between the electron donor and acceptor, a charge-separated state with very long life times is obtained upon light irradiation. The microscopic nanosheet segregation is actually quite helpful here since it also helps avoiding the photocatalytic degradation of the methyl viologen molecules by the niobate nanosheets.

As already mentioned several times in this article, the field of colloidal suspensions of nanosheets is much wider than that of clay platelets. Many of the experiments described here could be performed with other types of nanosheets and the most salient features of the behaviour of clay suspensions should also be observed with other plate-like nanoparticles.

Indeed, the research field of exfoliation of mineral or inorganic phases in aqueous or organic solvents is still in its infancy if one considers the very limited number of explored phases to date [84–87] compared to the very large number of two-dimensional solid-state materials reported so far. However, liquid-crystalline phases may or may not be observed, upon exfoliation, depending upon (i) the nature of the solvent; (ii) whether the inorganic two-dimensional molecular frame is fully preserved in solution; and (iii) its flexibility and charge. Indeed, various clues and suggestions about possible candidates for such new lyotropic liquid-crystalline phases based on mineral nanotubes and nanowires have already been proposed.[88] In a similar way, for colloidal suspensions of nanosheets, in addition to the mesophases of carbon-based, metal-oxide, and metal hydroxide materials that were already reported,[7–13,55,89–95] possible good candidates are metal chalcogenides of the MX_2 and M_2X_3 types (where M is a metal and X a chalcogen).[96] Other possible candidates are nitrides (BN) and phosphates ($VOPO_4$).[97–99] However, achieving good colloidal stability of such nanosheet suspensions, either by polymer grafting or through electrostatic repulsions, still represents a major hurdle. Provided that this step is properly mastered, then liquid-crystalline phases should be obtained with these systems upon increasing concentration.

Thanks to studies of model systems like clays or gibbsite, the main thermodynamic and structural features of colloidal suspensions of nanosheets are now rather well known. Nevertheless, remaining unsolved issues are the role of nanosheet flexibility and polydispersity and the detailed understanding of electrostatic interactions of anisotropic charged platelets in aqueous solvents. Moreover, from the more specific point of view of liquid crystals, with a few notable exceptions,[100] most of the dynamic properties of nanosheet suspensions still need to be investigated. Indeed,

extremely little is known about physical properties as basic as anchoring, elastic constants, viscosities, etc. Therefore, we believe that a large research domain is now opening up for experimental and theoretical investigations.

Acknowledgements

We gratefully acknowledge the French ANR for financial support under the ANR-07-BLANC-0194 program.

References

- [1] Onsager L. The effects of shape on the interaction of colloidal particles. *Ann NY Acad Sci.* 1949;51:627–659.
- [2] Vroege GJ, Lekkerkerker HNW. Phase-transitions in lyotropic colloidal and polymer liquid-crystals. *Rep Prog Phys.* 1992;55:1241–1309.
- [3] Gabriel JCP, Davidson P. New trends in colloidal liquid crystals based on mineral moieties. *Adv Mater.* 2000;12:9–20.
- [4] Davidson P, Gabriel JCP. Mineral liquid crystals. *Curr Opin Colloid Interface Sci.* 2005;9:377–383.
- [5] Castro Neto AH, Guinea F, Peres NMR, Novoselov KS, Geim AK. The electronic properties of graphene. *Rev Mod Phys.* 2009;81:109–162.
- [6] Geim AK. Graphene: status and prospects. *Science.* 2009;324:1530–1534.
- [7] Kim JE, Han TH, Lee SH, Kim JY, Ahn CW, Yun JM, Kim SO. Graphene oxide liquid crystals. *Angew Chem Int Edit.* 2011;50:3043–3047.
- [8] Guo F, Kim F, Han TH, Shenoy VB, Huang JX, Hurt RH. Hydration-responsive folding and unfolding in graphene oxide liquid crystal phases. *ACS Nano.* 2011;5:8019–8025.
- [9] Xu Z, Gao, C. Aqueous liquid crystals of graphene oxide. *ACS Nano.* 2011;5:2908–2915.
- [10] Xu Z, Gao, C. Graphene chiral liquid crystals and macroscopic assembled fibres. *Nat Commun.* 2011;2:571.
- [11] Dan B, Behabtu N, Martinez A, Evans JS, Kosynkin DV, Tour JM, Pasquali M, Smalyukh II. Liquid crystals of aqueous, giant graphene oxide flakes. *Soft Matter.* 2011;7:11154–11159.
- [12] Behabtu N, Lomeda JR, Green MJ, Higginbotham AL, Sinitiskii A, Kosynkin DV, Tsentelovich D, Parra-Vasquez ANG, Schmidt J, Kesselman E, Cohen Y, Talmon Y, Tour JM, Pasquali M. Spontaneous high-concentration dispersions and liquid crystals of graphene. *Nat Nanotechnol.* 2010;5:406–411.
- [13] Zamora-Ledezma C, Puech N, Zakri C, Grelet E, Moulton SE, Wallace GG, Gambhir S, Blanc C, Anglaret E, Poulin P. Liquid crystallinity and dimensions of surfactant-stabilized sheets of reduced graphene oxide. *J Phys Chem Lett.* 2012;3:2425–2430.
- [14] Zhang ZX, van Duijneveldt JS. Isotropic-nematic phase transition of nonaqueous suspensions of natural clay rods. *J Chem Phys.* 2006;124:154910.
- [15] Yasarawan N, van Duijneveldt JS. Dichroism in dye-doped colloidal liquid crystals. *Langmuir.* 2008;24:7184–7192.
- [16] Kajiwara K, Donkai N, Fujiyoshi Y, Inagaki H. Lyotropic mesophase of imogolite .2. Microscopic observation of imogolite mesophase. *Makromol Chem-Macromol Chem Phys.* 1986;187:2895–2907.
- [17] Kajiwara K, Donkai N, Hiragi Y, Inagaki H. Lyotropic mesophase of imogolite .1. Effect of polydispersity on phase-diagram. *Makromol Chem-Macromol Chem Phys.* 1986;187:2883–2893.
- [18] Donkai N, Hoshino H, Kajiwara K, Miyamoto T. Lyotropic mesophase of imogolite .3. Observation of liquid-crystal structure by scanning electron and novel polarized optical microscopy. *Makromol Chem-Macromol Chem Phys.* 1993;194:559–580.
- [19] Donkai N, Kajiwara K, Schmidt M, Miyamoto T. Lyotropic mesophase of imogolite – molecular-weight fractionation and polydispersity effect. *Makromol Chem-Rapid Commun.* 1993;14:611–617.
- [20] Levitz P, Zinsmeister M, Davidson P, Constantin D, Poncelet O. Intermittent Brownian dynamics over a rigid strand: heavily tailed relocation statistics in a simple geometry. *Phys Rev E.* 2008;78:030102.
- [21] Grim RE. *Clay mineralogy.* 2nd ed. New York: McGraw-Hill; 1968. p. 464.
- [22] Ross CS, Hendricks SB. Minerals of the montmorillonite group, their origin and relation to soils and clays. USGS Numbered Ser. 1945;205-B:23–79.
- [23] Freundlich H. Ueber thixotropie. *Kolloid Z.* 1928;46:289–307.
- [24] Langmuir I. The role of attractive and repulsive forces in the formation of tactoids, thixotropic gels, protein crystals and coacervates. *J Chem Phys.* 1938;6:873–896.
- [25] Broughton G, Squires L. The gelation of bentonite suspensions. *J Phys Chem.* 1936;40:1041–1053.
- [26] Van Olphen H. Rheological phenomena of clay sols in connection with the charge distribution on the micelles. *Discuss Faraday Soc.* 1951;11:82–84.
- [27] Norrish K. The swelling of montmorillonite. *Discuss Faraday Soc.* 1954;18:120–134.
- [28] Callaghan JC, Ottewill RH. Interparticle forces in montmorillonite gels. *Faraday Discuss.* 1974;57:110–118.
- [29] Ramsay JDF. Colloidal properties of synthetic hectorite clay dispersions .1. Rheology. *J Colloid Interface Sci.* 1986;109:441–447.
- [30] Mourchid A, Delville A, Lambard J, Lecolier E, Levitz P. Diagram of colloidal dispersions of anisotropic charged-particles – equilibrium properties, structure, and rheology of Laponite suspensions. *Langmuir.* 1995;11:1942–1950.
- [31] Mourchid A, Lecolier E, Van Damme H, Levitz P. On viscoelastic, birefringent, and swelling properties of Laponite clay suspensions: revisited phase diagram. *Langmuir.* 1998;14:4718–4723.
- [32] Knaebel A, Bellour M, Munch JP, Viasnoff V, Lequeux F, Harden JL. Aging behavior of Laponite clay particle suspensions. *Europhys Lett.* 2000;52:73–79.
- [33] Abou B, Bonn D, Meunier J. Aging dynamics in a colloidal glass. *Phys Rev E.* 2001;64:021510.
- [34] Bonn D, Kellay H, Tanaka H, Wegdam G, Meunier J. What is the difference between a gel and a glass? *Langmuir.* 1999;15:7534–7536.
- [35] Jabbari-Farouji S, Eiser E, Wegdam GH, Bonn D. Ageing dynamics of translational and rotational diffusion in a colloidal glass. *J Phys-Condens Mat.* 2004;16:L471–L477.
- [36] Michot LJ, Bihannic I, Porsch K, Maddi S, Baravian C, Mougél J, Levitz P. Phase diagrams of Wyoming Namontmorillonite clay. Influence of particle anisotropy. *Langmuir.* 2004;20:10829–10837.
- [37] Martin C, Pignon F, Magnin A, Meireles M, Lelievre V, Lindner P, Cabane B. Osmotic compression and expansion of highly ordered clay dispersions. *Langmuir.* 2006;22:4065–4075.
- [38] Martin C, Pignon F, Piau JM, Magnin A, Lindner P, Cabane B. Dissociation of thixotropic clay gels. *Phys Rev E.* 2002;66:021401.

- [39] Cocard S, Tassin JF, Nicolai T. Dynamical mechanical properties of gelling colloidal disks. *J Rheol.* 2000;44:585–594.
- [40] Joshi YM, Reddy GRK. Aging in a colloidal glass in creep flow: time-stress superposition. *Phys Rev E.* 2008;77:021501.
- [41] Paineau E, Antonova K, Baravian C, Bihannic I, Davidson P, Dozov I, Imperor-Clerc M, Levitz P, Madsen A, Meneau F, Michot LJ. Liquid-crystalline nematic phase in aqueous suspensions of a disk-shaped natural beidellite clay. *J Phys Chem B.* 2009;113:15858–15869.
- [42] Miyamoto N, Nakato T. Liquid crystalline nanosheet colloids with controlled particle size obtained by exfoliating single crystal of layered niobate K₄Nb₆O₁₇. *J Phys Chem B.* 2004;108:6152–6159.
- [43] Michot LJ, Bihannic I, Pelletier M, Rinnert E, Robert JL. Hydration and swelling of synthetic Na-saponites: influence of layer charge. *Am Mineral.* 2005;90:166–172.
- [44] Michot LJ, Bihannic I, Maddi S, Funari SS, Baravian C, Levitz P, Davidson P. Liquid-crystalline aqueous clay suspensions. *Proc Nat Acad Sci U.S.A.* 2006;103:16101–16104.
- [45] Michot LJ, Bihannic I, Maddi S, Baravian C, Levitz P, Davidson P. Sol/gel and isotropic/nematic transitions in aqueous suspensions of natural nontronite clay. Influence of particle anisotropy. 1. Features of the I/N transition. *Langmuir.* 2008;24:3127–3139.
- [46] DiMasi E, Fossum JO, Gog T, Venkataraman C. Orientational order in gravity dispersed clay colloids: a synchrotron x-ray scattering study of Na fluorohectorite suspensions. *Phys Rev E.* 2001;64:061704.
- [47] Zocher HZ. Ueber freiwillige strukturbildung in solen. *Anorg Allg Chem.* 1925;147:91–110.
- [48] Ringdal NI, Fonseca DM, Hansen EL, Hemmen H, Fossum JO. Nematic textures in colloidal dispersions of Na-fluorohectorite synthetic clay. *Phys Rev E.* 2010;81:041702.
- [49] Eppenga R, Frenkel D. Monte-Carlo study of the isotropic and nematic phases of infinitely thin hard platelets. *Mol Phys.* 1984;52:1303–1334.
- [50] Bates MA, Frenkel D. Influence of polydispersity on the phase behavior of colloidal liquid crystals: a Monte Carlo simulation study. *J Chem Phys.* 1998;109:6193–6199.
- [51] Bates MA, Frenkel D. Nematic-isotropic transition in polydisperse systems of infinitely thin hard platelets. *J Chem Phys.* 1999;110:6553–6559.
- [52] Agra R, Trizac E, Bocquet L. The interplay between screening properties and colloid anisotropy: towards a reliable pair potential for disc-like charged particles. *Eur Phys J E.* 2004;15:345–357.
- [53] Morales-Anda L, Wensink HH, Galindo A, Gil-Villegas A. Anomalous columnar order of charged colloidal platelets. *J Chem Phys.* 2012;136:034901.
- [54] van der Kooij FM, Kassapidou K, Lekkerkerker HNW. Liquid crystal phase transitions in suspensions of polydisperse plate-like particles. *Nature.* 2000;406:868–871.
- [55] Gabriel JCP, Camerel F, Lemaire BJ, Desvaux H, Davidson P, Batail P. Swollen liquid-crystalline lamellar phase based on extended solid-like sheets. *Nature.* 2001;413:504–508.
- [56] Gabriel JCP, Sanchez C, Davidson P. Observation of nematic liquid-crystal textures in aqueous gels of smectite clays. *J Phys Chem.* 1996;100:11139–11143.
- [57] Paineau E, Bihannic I, Baravian C, Philippe AM, Davidson P, Levitz P, Funari SS, Rochas C, Michot LJ. Aqueous suspensions of natural swelling clay minerals. 1. Structure and electrostatic interactions. *Langmuir.* 2011;27:5562–5573.
- [58] De Gennes PG. *The Physics of liquid crystals.* Oxford: Clarendon Press; 1974.
- [59] Yamaguchi D, Miyamoto N, Fujita T, Nakato T, Koizumi S, Ohta N, Yagi N, Hashimoto T. Aspect-ratio-dependent phase transitions and concentration fluctuations in aqueous colloidal dispersions of charged platelike particles. *Phys Rev E.* 2012;85:011403.
- [60] Brown ABD, Rennie AR. Monodisperse colloidal plates under shear. *Phys Rev E.* 2000;62:851–862.
- [61] Clarke SM, Rennie AR, Convert P. A diffraction technique to investigate the orientational alignment of anisotropic particles: studies of clay under flow. *Europhys Lett.* 1996;35:233–238.
- [62] van der Beek D, Davidson P, Wensink HH, Vroege GJ, Lekkerkerker HNW. Influence of a magnetic field on the nematic phase of hard colloidal platelets. *Physical Review E.* 2008;77:031708.
- [63] Hemmen H, Ringdal NI, De Azevedo EN, Engelsberg M, Hansen EL, Meheust Y, Fossum JO, Knudsen KD. The Isotropic-nematic interface in suspensions of Na-fluorohectorite synthetic clay. *Langmuir.* 2009;25:12507–12515.
- [64] Reich H, Schmidt M. Capillary nematization of hard colloidal platelets confined between two parallel hard walls. *J Phys-Condens Mat.* 2007;19:326103.
- [65] Bawden FC, Pirie NW, Bernal JD, Fankuchen I. Liquid-crystalline substances from virus-infected plants. *Nat Commun.* 1936;138:1051–1052.
- [66] Srajer G, Fraden S, Meyer RB. Field-induced nonequilibrium periodic structures in nematic liquid-crystals – nonlinear study of the twist Frederiks transition. *Phys Rev A.* 1989;39:4828–4834.
- [67] Hurd AJ, Fraden S, Lonberg F, Meyer RB. Field-induced transient periodic structures in nematic liquid-crystals - the splay Frederiks transition. *J Phys.* 1985;46:905–917.
- [68] Fraden S, Hurd AJ, Meyer RB, Cahoon M, Caspar DLD. Magnetic-field induced alignment and instabilities in ordered colloids of tobacco mosaic-virus. *J Phys.* 1985;46:85–113.
- [69] Lonberg F, Fraden S, Hurd AJ, Meyer RE. Field-induced transient periodic structures in nematic liquid-crystals – the twist-Freedericksz transition. *Phys Rev Lett.* 1984;52:1903–1906.
- [70] Connolly J, van Duijneveldt JS, Klein S, Pizzey C, Richardson RM. Manipulation of modified clay particles in a nematic solvent by a magnetic field. *J Phys-Condens Mat.* 2007;19:156103.
- [71] Dozov I, Paineau E, Davidson P, Antonova K, Baravian C, Bihannic I, Michot LJ. Electric-field-induced perfect anti-nematic order in isotropic aqueous suspensions of a natural beidellite clay. *J Phys Chem B.* 2011;115:7751–7765.
- [72] Nakato T, Nakamura K, Shimada Y, Shido Y, Houryu T, Iimura Y, Miyata H. Electrooptic response of colloidal liquid crystals of inorganic oxide nanosheets prepared by exfoliation of a layered niobate. *J Phys Chem C.* 2011;115:8934–8939.
- [73] Fossum JO, Meheust Y, Parmar KPS, Knudsen KD, Maloy KJ, Fonseca DM. Intercalation-enhanced electric polarization and chain formation of nano-layered particles. *Europhys Lett.* 2006;74:438–444.
- [74] Safinya CR, Sirota EB, Bruinsma RF, Jeppesen C, Plano RJ, Wenzel LJ. Structure of membrane surfactant and liquid-crystalline smectic lamellar phases under flow. *Science.* 1993;261:588–591.
- [75] Paineau E, Michot LJ, Bihannic I, Baravian C. Aqueous suspensions of natural swelling clay minerals. 2. Rheological characterization. *Langmuir.* 2011;27:7806–7819.

- [76] Philippe AM, Baravian C, Bezuglyy V, Angilella JR, Meneau F, Bihannic I, Michot LJ. Rheological study of two-dimensional very anisometric colloidal particle suspensions: from shear-induced orientation to viscous dissipation. *Langmuir*. 2013;29:5315–5324.
- [77] Kojima Y, Fukumori K, Usuki A, Okada A, Kurauchi T. Gas permeabilities in rubber clay hybrid. *J Mater Sci Lett*. 1993;12:889–890.
- [78] Paineau E, Dozov I, Bihannic I, Baravian C, Krapf MEM, Philippe AM, Rouziere S, Michot LJ, Davidson P. Tailoring highly oriented and micropatterned clay/polymer nanocomposites by applying an a.c. electric field. *ACS Appl Mater Inter*. 2012;4:4296–4301.
- [79] Koerner H, Hampton E, Dean D, Turgut Z, Drummy L, Mirau P, Vaia R. Generating triaxial reinforced epoxy/montmorillonite nanocomposites with uniaxial magnetic fields. *Chem Mater*. 2005;17:1990–1996.
- [80] Koerner H, Jacobs D, Tomlin DW, Busbee JD, Vaia RD. Tuning polymer nanocomposite morphology: AC electric field manipulation of epoxy-montmorillonite (clay) suspensions. *Adv Mater*. 2004;16:297–302.
- [81] Camerel F, Gabriel JCR, Batail P. Magnetically induced large mesoporous single-domain monoliths using a mineral liquid crystal as a template. *Adv Funct Mater*. 2003;13:377–381.
- [82] Miyamoto N, Yamada Y, Koizumi S, Nakato T. Extremely stable photoinduced charge separation in a colloidal system composed of semiconducting niobate and clay nanosheets. *Angew Chem Int Ed*. 2007;46:4123–4127.
- [83] Nakato T, Yamada Y, Miyamoto N. Photoinduced charge separation in a colloidal system of exfoliated layered semiconductor controlled by coexisting aluminosilicate clay. *J Phys Chem B*. 2009;113:1323–1331.
- [84] Batail P, Ouahab L, Penicaud A, Lenoir C, Perrin A. Preparation of the tetrabutylammonium salt of a rhenium(III) chalcogenide molecular cluster, $(C_4H_9)_4N[Re_6Se_5Cl_9]$ – access to the solution-phase chemistry of an analogous molybdenum chalcogenide, examples of electrochemical association with tetrathia (selena) fulvalene-based cationic radicals. *Cr Acad Sci II*. 1987;304:1111–1116.
- [85] Gabriel JCP, Boubekour K, Uriel S, Batail P. Chemistry of hexanuclear rhenium chalcogenide clusters. *Chem Rev*. 2001;101:2037–2066.
- [86] Osada M, Sasaki T. Exfoliated oxide nanosheets: new solution to nanoelectronics. *J Mater Chem*. 2009;19:2503–2511.
- [87] Ida S, Ogata C, Eguchi M, Youngblood WJ, Malouk TE, Matsumoto Y. Photoluminescence of perovskite nanosheets prepared by exfoliation of layered oxides, $K(2)Ln(2)Ti(3)O(10)$, $KLnNb(2)O(7)$, and $RbLnTa(2)O(7)$ (Ln: lanthanide ion). *J Am Chem Soc*. 2008;130:7052–7059.
- [88] Gabriel JCP, Davidson P. Mineral liquid crystals from self-assembly of anisotropic nanosystems. *Colloid Chem I*. 2003;226:119–172.
- [89] Miyamoto N, Nakato T. Liquid crystalline inorganic nanosheet colloids derived from layered materials. *Isr J Chem*. 2012;52:881–894.
- [90] Geng F, Ma R, Nakamura A, Akatsuka K, Ebina Y, Yamauchi Y, Miyamoto N, Tateyama Y, Sasaki T. Unusually stable ~ 100 -fold reversible and instantaneous swelling of inorganic layered materials. *Nat Commun*. 2013;4:1632.
- [91] Liu SY, Zhang J, Wang N, Liu WR, Zhang CG, Sun DJ. Liquid-crystalline phases of colloidal dispersions of layered double hydroxides. *Chem Mater*. 2003;15:3240–3241.
- [92] Zhang J, Luan LY, Zhu WX, Liu SY, Sun DJ. Phase behavior of aqueous suspensions of Mg_2Al layered double hydroxide: the competition among nematic ordering, sedimentation, and gelation. *Langmuir*. 2007;23:5331–5337.
- [93] Mourad MCD, Devid EJ, van Schooneveld MM, Vonk C, Lekkerkerker HNW. Formation of nematic liquid crystals of sterically stabilized layered double hydroxide platelets. *J Phys Chem B*. 2008;112:10142–10152.
- [94] Miyamoto N, Yamamoto S, Shimasaki K, Harada K, Yamauchi Y. Exfoliated nanosheets of layered perovskite $KCa_2Nb_3O_{10}$ as an inorganic liquid crystal. *Chem-Asian J*. 2011;6:2936–2939.
- [95] Liu ZP, Ma RZ, Osada M, Takada K, Sasaki T. Selective and controlled synthesis of α - and β -cobalt hydroxides in highly developed hexagonal platelets. *J Am Chem Soc*. 2005;127:13869–13874.
- [96] Coleman JN, Lotya M, O'Neill A, Bergin SD, King PJ, Khan U, Young K, Gaucher A, De S, Smith RJ, Shvets IV, Arora SK, Stanton G, Kim HY, Lee K, Kim GT, Duesberg GS, Hallam T, Boland JJ, Wang JJ, Donegan JF, Grunlan JC, Moriarty G, Shmeliov A, Nicholls RJ, Perkins JM, Grievson EM, Theuwissen K, McComb DW, Nellist PD, Nicolosi V. Two-dimensional nanosheets produced by liquid exfoliation of layered materials. *Science*. 2011;331:568–571.
- [97] Tanaka H, Ishida K, Okumiya T, Murakami M. Preparation and exfoliation of layered titanium butyl phosphates. *Colloid Polym Sci*. 2010;288:1427–1433.
- [98] Sun DZ, Sue HJ, Cheng ZD, Martinez-Raton Y, Velasco E. Stable smectic phase in suspensions of polydisperse colloidal platelets with identical thickness. *Phys Rev E*. 2009;80:041704.
- [99] Alberti G, Cavalaglio S, Dionigi C, Marmottini F. Formation of aqueous colloidal dispersions of exfoliated gamma-zirconium phosphate by intercalation of short alkylamines. *Langmuir*. 2000;16:7663–7668.
- [100] de Azevedo EN, Engelsberg M. Strongly damped dynamics of nematically ordered colloidal clay platelets in a magnetic field. *Langmuir*. 2009;25:1175–1180.